Inorganic Chemistry

pubs.acs.org/IC

Article

More-Is-Better Strategy for Constructing Homoligand Polypyridyl Ruthenium Complexes as Photosensitizers for Infrared Two-Photon Photodynamic Therapy

Shi-Jie Tang, Meng-Fan Wang, Rong Yang, Meng Liu, Qing-Fang Li, and Feng Gao*

Cite This: *Inorg. Chem.* 2023, 62, 8210−8218

Read Online

ACCESS | Metrics & More | Article Recommendations | Supporting Information

ABSTRACT: Photodynamic therapy (PDT) uses a combination of photosensitizers (PSs), light sources, and reactive oxygen species (ROS) to damage only the desired target and keep normal tissues from being hurt. The dark cytotoxicity (chemotoxicity) of PSs, leading to whole-body damage in the absence of irradiation, is a major limiting factor in PDT. How to simultaneously increase ROS generation and decrease dark cytotoxicity is an essential challenge that must be resolved in PS research. In this study, a series of homoligand polypyridyl ruthenium complexes (HPRCs) containing three singlet oxygen ($^1O_2$)-generating ligands (L) in a single molecule ($[Ru(L)_3]^{2+}$) have been constructed. Compared to the heteroligand complexes $[Ru(bpy)_2(L)]^{2+}$ where bpy is 2,2′-bipyridine, the $^1O_2$ quantum yield under infrared two-photon irradiation and the DNA photocleavage effect of the HPRCs are significantly enhanced with two more ligands L. The intraligand triplet excited states transition played an important role in the activation of oxygen. The HPRCs target the mitochondria but not the nuclei, generating $^1O_2$ intracellularly under irradiation of visible or infrared light. **Ru1** exhibits high phototoxicity and low dark cytotoxicity toward human malignant melanoma cells in vitro. Moreover, HPRCs have minimal cytotoxicity to human normal liver cells, suggesting their potential as antitumor PDT reagents with more security. This study may provide inspiration for the structural design of potent PS for PDT.

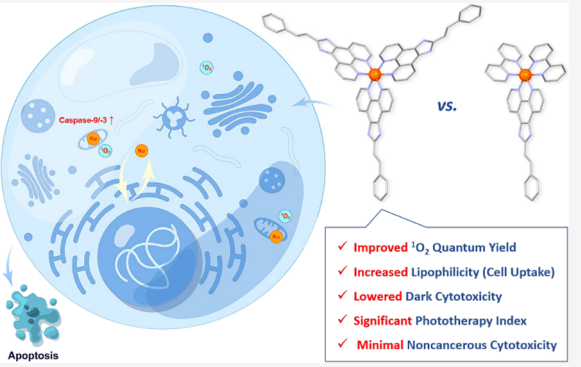

1. INTRODUCTION

Surgical, chemotherapeutic, and radiation therapies are commonly applied in cancer treatments. However, these technics have certain disadvantages, including invasiveness, a high recurrence rate, substantial systemic toxicity, and side effects.[1,2] Photodynamic therapy (PDT) is an alternative to chemotherapy, which mainly depends on a photosensitizer (PS), oxygen molecules, and a light source. The PSs are innoxious to cells or tissues without irradiation and only work in the tumor area exposing to light, thus have a low risk of side effects. The PS is first excited by light from the ground state (GS, S_0) to singlet excited states (^{1}ESs) and subsequently relaxes from higher^{1}ESs (S_n, $n > 1$) to S_1 through internal conversion (IC) and transfers from^{1}ESs to more stable triplet ESs (^{3}ESs) by intersystem crossing (ISC).[2] The PS in ^{3}ESs can produce ROS by ES electron transfer/hydrogen atom abstraction (Type I) or generate highly active singlet oxygen ($^1O_2$) by ES energy transfer (Type II). The light-generated ROS, notably $^1O_2$, can react with biological targets such as lipids, proteins, and nucleic acids, destroy the targeted cells, damage the vasculature associated with the tumor, and stimulate antitumor immunity.[3−6] Consequently, the characteristic of ^{3}ES and the ROS quantum yield are two crucial aspects of a PS.

Many Ru(II) complexes have been successfully developed as PSs in PDT and photochemotherapy (PCT) for their long ^{3}ES lifetimes and high $^1O_2$ quantum yields (Φ_Δ).[7,8] Although some good Ru(II)-PSs like TLD1433, which entered a clinical trial in 2018, can be excited by red light (better than traditional blue light), even longer excitation wavelength, especially the infrared (IR) light, will be more practical for a deeper (typically >1 cm) and safer PDT. Ru(II), Ir(III), and Os(II) complexes with distinct IR two-photon absorption (TPA) have exhibited versatile properties in antitumor phototherapy.[7,9−13] Currently, the two-photon (TP) excitation depends on lasers with extremely high energy density. The power exceeds the maximum allowable exposure value (0.33 W cm^{-2}) under IR laser for human skin (ANSI Z136.1-2014). In addition, the high-power laser beam's restricted light spot size makes it hard to cover the solid tumors entirely, which severely limits its applicability and

Received: February 21, 2023
Published: May 17, 2023

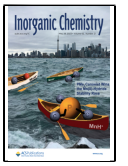

https://doi.org/10.1021/acs.inorgchem.3c00585
Inorg. Chem. 2023, 62, 8210−8218

efficiency. As another option, the high-power xenon lamp with high exposure usually causes damage to the tumor's surrounding tissues due to its extensive irradiation area.

Recently, we designed a dinuclear Ru(II) complex[12] with remarkable TPA cross-section (TPACSs, σ) and photothermal conversion efficiency (PCE) in the IR region and realized its dual PDT and photothermal therapy (PTT) in vivo by using a low-power laser (LPL, 808 nm, 100 mW cm^{-2}) with a tunable beam diameter (>1.0 cm) which has demonstrated good applicability in the antitumor phototherapy of upconverting nanoparticles.[14] Exploring promising Ru(II)-PSs with simpler structures and similar high phototherapy indexes (PIs) will undoubtedly be beneficial to pharmaceutical manufacturing. In a previous study, a ligand sip (Figure 1) has shown a high Φ_Δ

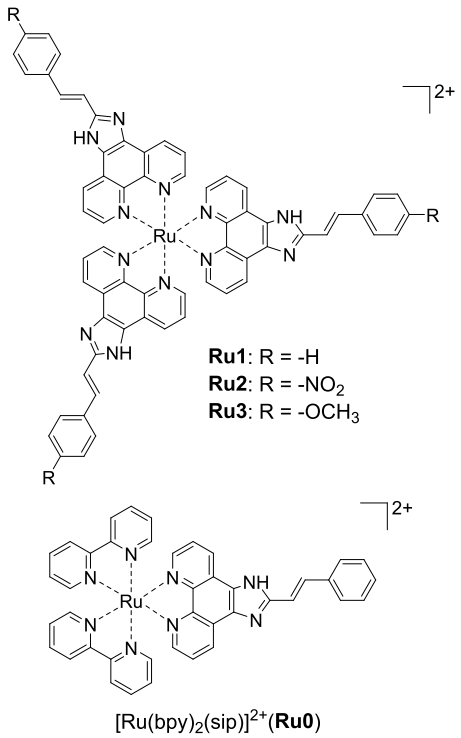

Figure 1. Homoligand polypyridyl ruthenium complexes **Ru1**−**Ru3** designed in this work and previous heteroligand complex $[Ru(bpy)_2(sip)]^{2+}$(**Ru0**).

value. The Ir(III) complex of sip has negligible DNA affinity and very low dark cytotoxicity and serves as a potent PS with high PI.[15] However, its Ru(II) analog **Ru0** (Figure 1) is unlikely to be a PS for PDT even though it shows remarkable photocytotoxicity, due to its nonignorable chemotoxicity (dark cytotoxicity).[16]

In this study, three homoligand polypyridyl Ru(II) complexes (HPRCs) containing three sip-type ligands in a single molecule ($[Ru(L)_3]^{2+}$) have been constructed (**Ru1**−**Ru3**, Figure 1). The light-induced Φ_Δ and the DNA photocleavage effect of HPRCs are anticipated to be significantly enhanced, compared with the parent complex **Ru0** due to the increased number of highly efficient $^1O_2$-generating ligand sip. The DNA affinity of HPRC is expected to reduce greatly as the steric hindrance of the two external ligands became unignorable when one ligand attempts to insert itself into DNA. Their increased lipophilicity is found to be beneficial for more efficient cell uptake. The HPRCs have shown remarkable in vitro phototherapy indexes to human malignant melanoma cells under irradiation of visible (450 nm) and IR (808 nm) light and very low toxicity to human normal liver cells. We anticipate that our study will spark interest among researchers in HPRC-type PSs and give meaningful strategies for PS design in antitumor PDT.

2. EXPERIMENTAL SECTION

2.1. Materials. Ruthenium chloride ($RuCl_3$), potassium hexafluorophosphate (KPF_6), ethylene glycol, *N*-ethyl-morpholine, neutral alumina (200−300 mesh), and organic solvents were purchased from Adamas. Ammonium acetate, propanoic acid, aqueous ammonia, $CDCl_3$, and DMSO-d_6 were purchased from Energy Chemical.

2.2. Cell Lines and Culture Conditions. Human malignant melanoma A375 and normal liver HL-7702 cell lines (STR authentication, Animal Research and Resource Center) were cultured in RPMI 1640 medium (Adamas Life) supplemented with 10% (v/v) FBS (Gibco BRL) at 37 °C in a carbon dioxide incubator (95% air and 5% CO_2) with a humidified atmosphere. The tumor cells were routinely subcultured twice per week by trypsin−EDTA treatment. The cells in an exponential growth phase were harvested and counted for tumor inoculation.

2.3. Subcellular Colocalization. A375 cells were grown on an 8-Chamber Glass Slide (Thermo Fisher Scientific) at a density of 6×10^4 cell ml^{-1} and incubated for 1 h with the HPRCs at 2.5 μM. The cells were washed with PBS twice. Nuclei and mitochondria were counterstained with Hoechst 33342 (Invitrogen) and MitoTracker Green (MTG, Invitrogen), respectively. Luminescence images were collected on a Leica TCS SP8 DIVE two-photon confocal laser scanning microscopy (CLSM) at three detection channels (MTG: λ_{ex} = 488 nm, λ_{em} = 510−520 nm; HPRC: λ_{ex} = 808 nm, λ_{em} = 610−650 nm; Hoechst: λ_{ex} = 405 nm, λ_{em} = 460−500 nm) and processed by LAS X (Leica) software.

2.4. Cell Uptake. Exponentially growing A375 cells (2×10^7 cell ml^{-1}) were harvested, and the resulting single-cell suspension was plated into 100 mm tissue culture plates (Adamas). After 24 h of incubation (37 °C, 5% CO_2), the cells were incubated with 5 μM HPRC for 2 h at 37 °C in RPMI 1640 medium with 10% (v/v) FBS. The cells were rinsed with PBS, detached with trypsin, counted and divided into three portions: (1) in portion 1, the nuclei were extracted using a nucleus extraction kit (Thermo); (2) in portion 2, the cytoplasm was extracted using a cytoplasm extraction kit (Thermo); and (3) in portion 3, the mitochondria were extracted using a mitochondrial extraction kit (Thermo). All extraction procedures followed the manufacturer's protocols. To verify the HPRC concentration-dependent cell uptake, the same amount of A375 cells was incubated with 5, 50, and 200 μM of HPRC for 2 h at 37 °C in RPMI 1640 medium with 10% (v/v) FBS and 5% DMSO. The samples were digested with 60% HNO_3 at room temperature for 1 day. Each sample was diluted with water to obtain 2% HNO_3 sample solutions. The ruthenium content was measured by a PlasmaQuant PQ9000 inductively coupled plasma mass spectrometry (ICP-MS).

2.5. Intracellular Singlet Oxygen Generation. 2′,7′-Dichlorodihydrofluorescein diacetate (DCFH-DA, Thermo) was used as a fluorescent probe to detect the intracellularly generated ROS. A375 cells were seeded in a cell culture dish. After 24 h of incubation (37 °C, 5% CO_2), the cells were incubated with HPRC solution (5 μM) in the absence and presence of ABDA (100 μM) for 2 h at 37 °C. After rinsing with PBS, the cells were incubated with DCFH-DA (10 μM) for 20 min, washed with 3 × 1 mL PBS, irradiated with a 450 nm LED array (50 mW cm^{-2}) or an 808 nm LPL (100 mW cm^{-2}) for 5 min, and photographed by CLSM as described above.

2.6. In Vitro Cell Viability (CCK-8 Assay). The cell viability was determined by the CCK-8 assay. For cytotoxicity to A375 cells, exponentially grown cells were seeded in 384-well plates, followed by a 24 h incubation for attachment. Cells were incubated with different concentrations of HPRCs or cisplatin. For phototoxicity studies, after 12 h of incubation, the supernatant was replaced with fresh culture medium and cells were subjected to irradiation by the 450 nm LED array (50 mW cm^{-2}, light dose = 30.0 J cm^{-2}) and 808 nm LPL (100

https://doi.org/10.1021/acs.inorgchem.3c00585
Inorg. Chem. 2023, 62, 8210−8218

mW cm^{-2}, light dose = 30.0 J cm^{-2}) and incubated for an additional 48 h. Cells without irradiation were replaced with a fresh culture medium and maintained in the dark. Then, 10 μL of CCK-8 (Adamas Life) working solution was added and incubated for 1 h. Absorbance at 450 nm was measured on an iMark (Bio-rad) microplate reader, before and after CCK-8 incubation. Data were reported as the mean ± standard deviation (n = 3). IC_{50} values were determined by plotting the percentage of viability versus concentration on a logarithmic graph. For cytotoxicity to normal cells, exponentially grown HL-7702 cells were used instead.

2.7. Apoptosis Assay by Flow Cytometry Analysis. Cell apoptosis was measured by Annexin V-FITC (fluorescein isothiocyanate, AV) and propidium iodide (PI) based on the manufacturer's manual (Beyotime). Human melanoma cells A375 at a density of 1 × 10^5 cell mL^{-1} in 1 mL of RPMI 1640 medium containing 10% FBS and 1 × 10^3 units penicillin/streptomycin were incubated with 1 μM of HPRC at 37 °C (5% CO_2) for 2 h. The HPRC-containing medium was replaced with a fresh HPRC-free medium. Cells were irradiated by the 450 nm LED array (50 mW cm^{-2}, light dose = 30.0 J cm^{-2}), 808 nm LPL (100 mW cm^{-2}, light dose = 30.0 J cm^{-2}) or away from the light for 10 min at room temperature, stained with AV/PI or AV alone, and immediately examined with a BD FACSCalibur flow cytometer via two channels or single channel.

2.8. Caspase Activation. Caspase-3 and -9 activities were measured through cleavage of a colorless substrate specific for caspase-3 (Ac-DEVD-*p*NA) or caspase-9 (Ac-LEHD-*p*NA) releasing *p*-nitroaniline (*p*NA). A375 cells were seeded in 96-well plates (1 × 10^5 cells/well) and allowed to incubate for 6 h. The cells were then incubated respectively with control (PBS) or HPRC in the dark. After 12 h incubation, the cells were divided into two groups. The dark groups were incubated for an additional 12 h, and the irradiation groups were exposed to 808 nm LPL (100 mW cm^{-2}, light dose = 30.0 J cm^{-2}) before they were incubated for 12 h in the dark. The cells were lysed and treated with a caspase-3 or -9 activity kit (Beyotime) according to the manufacturer's protocol. Absorbance at 405 nm was measured on an iMark (Bio-rad) microplate reader. The caspase-3 and -9 activities in drug-treated cells were determined as relative values to control groups (PBS). Data were reported as the mean ± standard deviation (n = 3).

3. RESULTS AND DISCUSSION

3.1. Synthesis and Photostability. The synthesis of **Ru1**−**Ru3** and their characterization, including ^{1}H NMR (Figure S1), ^{13}C NMR, ESI-MS, and microanalysis, are shown in the Supporting Information. In comparison to Cl-coordinated Ru(II)-arene complexes, coordination-saturated PRCs are known to be inert to ligand substitution.[17,18] By examining the absorption spectral changes of Ru(II) complexes in the absence of light, no hydrolysis was observed for **Ru1**−**Ru3** in the aqueous solution (Tris−HCl buffer, Figure S2) or RPMI 1640 cell culture medium (Figure S3). Upon light irradiation with a 450 nm LED (50 mW cm^{-2}) or an 808 nm LPL (100 mW cm^{-2}), **Ru1**−**Ru3** are also stable, as the spectra showed nearly no change in the MLCT bands.

3.2. Spectroscopy and DFT Calculations. The absorption spectra of **Ru1**−**Ru3** (10 μM) were recorded in the acetonitrile solution (Figure 2), and the absorption band maxima (λ_{abs}) and molar extinction coefficients (ε) are listed in Table 1. In the range of 400−480 nm, absorption bands were attributed to the metal-to-ligand charge transfer (MLCT, d_{Ru} to π_L*) transitions,[19,20] as shown in the simulated absorption spectra (Figures 3a and S4) by TDDFT, the simplified Jablonski diagraph (Figure 3b) and the real space representation of hole and electron distributions (Figures 3c, S5, and S6). Bands between 350 and 400 nm are attributed to the ligand-centered (LC, π_L to π_L*) transitions, as in **Ru0** and its analogs.[16]

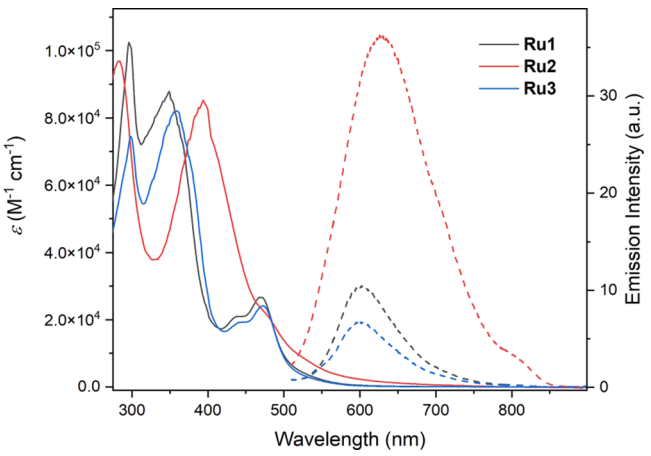

Figure 2. Absorption (solid) and emission spectra (dashed, λ_{ex} = 455 nm) of **Ru1**−**Ru3** (10 μM) in anhydrous acetonitrile at 20 °C.

Table 1. Spectroscopy and Electrochemistry Data for HPRCs Ru1−**Ru3**

HPRC	λ_{abs}/nm (ε/×10^4 M^{-1} cm^{-1})	λ_{em}/nm	Φ/%	E_{ox}/V	E_{red}/V
Ru1	471 (2.68), 437 (2.08), 348 (8.80), 296 (10.24)	603	0.63	0.71	−1.38, −1.56, −2.06
Ru2	474 (2.23), 393 (8.20), 282 (9.68)	626	2.8	0.72	−1.31, −1.52, −2.09
Ru3	472 (2.40), 441 (1.93), 359 (8.20), 298 (7.43)	600	0.41	0.65	−1.39, −1.50, −2.08

The emission spectra of **Ru1**−**Ru3** exhibited typical characteristics for Ru(II) complexes (Figure 2), with emission band maxima focused around 610 nm (Table 1). From the quantum yields of emission (Φ) in anhydrous MeCN, the emission intensity of **Ru2** (Φ = 0.028) is quite moderate, compared with the reference $[Ru(bpy)_3]^{2+}$ (Φ = 0.095 in MeCN). **Ru1** and **Ru3** emit even fainter. In an aqueous solution, all HPRCs are nearly nonemitting (<5 μM) through one-photon^{1}MLCT excitation due to the quenching of water molecules. Theoretical analysis revealed that the emission of HPRCs arose from the intraligand (^{3}IL) transition (Figures 3b,c, S5, and S6). A low-energy ^{3}IL state is suggested to be a significant factor for the $^1O_2$ production of a transition metal-based PS, such as TLD1433.[8] Therefore, the above studies on the ES properties of HPRCs elucidated plausible implications for their good performances in PDT.

3.3. Electrochemistry. The GS oxidative and reductive potentials (E_{ox} and E_{red}) of **Ru1**−**Ru3** were studied in degassed anhydrous CH_3CN by CV and summarized in Table 1. **Ru1**−**Ru3** exhibited irreversible couples ranging from 0.65 to 0.72 V, which were attributed to Ru(III)/Ru(II) oxidation.[21,22] Due to the presence of the electron-withdrawing $-NO_2$ group, the electron-accepting ability of **Ru2** is enhanced, and its oxidation potential is shifted toward the anode compared to **Ru1**. The oxidation potential of **Ru3** moves to the cathode due primarily to the function of electron-donating groups. Three reduction couples (−1.31 to −1.39, −1.50 to −1.57, and −2.06 to −2.09 V) representing the reduction with sip as the core were observed for **Ru1**−**Ru3**, and the redox potentials are comparable to those of previously reported sip-containing complexes.

3.4. Singlet Oxygen Quantum Yield. The $^1O_2$ quantum yields (Φ_Δ, Table 2) for each HPRC and **Ru0**, as well as

https://doi.org/10.1021/acs.inorgchem.3c00585
Inorg. Chem. 2023, 62, 8210−8218

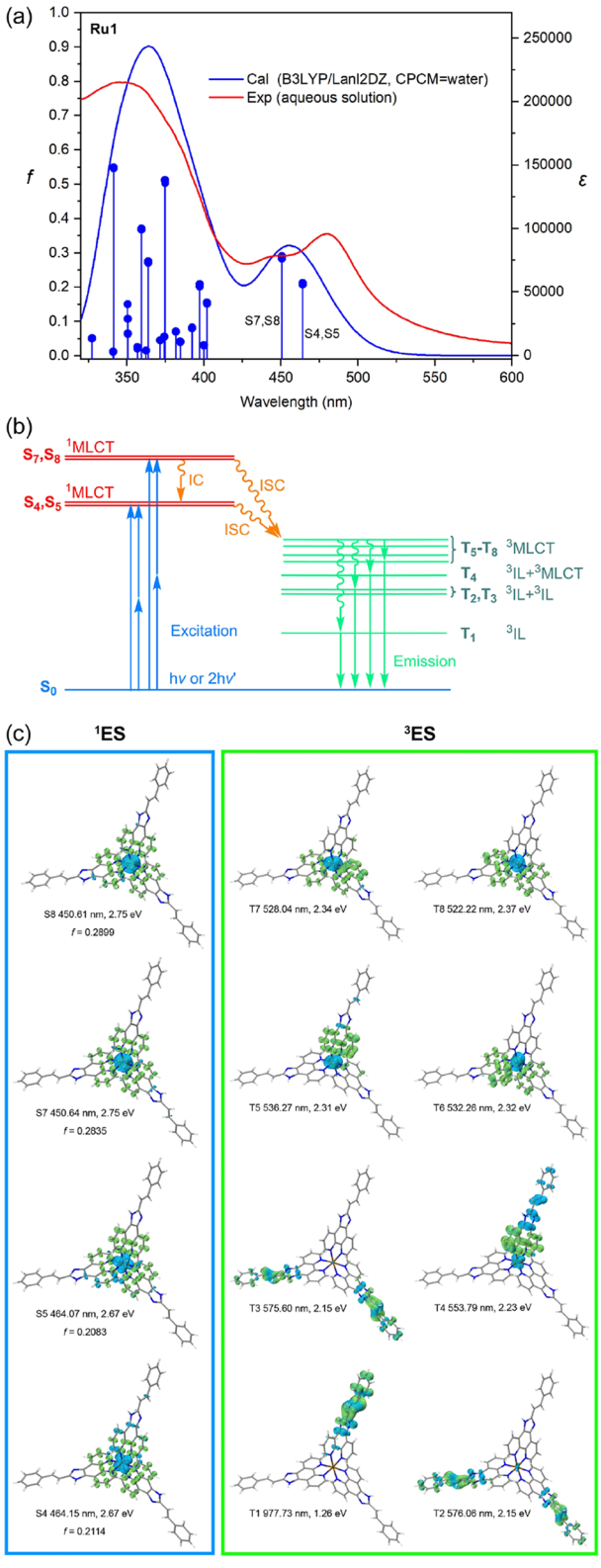

Figure 3. Electron transition analysis of **Ru1** by quantum chemistry theoretical calculations (B3LYP/Lanl2DZ, CPCM = water). (a) Experimental and calculated absorption spectra of **Ru1**. (b) Simplified Jablonski diagraph showing the excitation, emission, and energy transfer of **Ru1**. (c) Hole (blue) and electron (green) distributions of **Ru1** for the excited singlet (^{1}ES) and triplet states (^{3}ES). Excitation wavelength (nm), excitation energy (eV), and oscillator strength (f) for each transition are included.

$[Ru(bpy)_3]^{2+}$ (**Ref**), were determined by the absorbance variations of ABDA at 378 nm (Figures 4, and S7−S9). Upon irradiation of 450 nm LED (50 mW cm^{-2}), the $\Phi_{\Delta 450}$ values for **Ru1** and **Ru3** were 0.59 and 0.49, respectively, suggesting a high $^1O_2$ generation efficiency. Compared to **Ru0** (0.13), the $\Phi_{\Delta 450}$ of **Ru1** increased approximately fourfold, showing that substituting the two bpy ligands with sip can significantly boost the $^1O_2$ production of the Ru(II) complex, which has a substantial effect on the efficacy of PDT. Under 808 nm LPL (100 mW cm^{-2}) irradiation, **Ru1** also has the highest $\Phi_{\Delta 808}$ value among these complexes. This can be rationalized from two aspects. On the one hand, as shown in the TDDFT calculations and real space distributions of ES (Figures S2−S4), all the lowest three ^{3}ESs are ^{3}IL transitions for each HPRC, which support a high PDT capacity.[23,24] On the other hand, **Ru1** exhibited a lower ^{3}IL energy level than **Ru2** and **Ru3** (Figures 3c, S2, and S3), implying a more efficient intersystem crossing (ISC) pathway to reach the ^{3}ES which is responsible for energy transfer in type II PDT.[25] The high $^1O_2$ quantum yield of **Ru1**−**Ru3** may lead to enhanced DNA photocleavage and phototoxicity. Since no IR absorption of the HPRCs was observed in the absorption spectra, the origin of good exciting efficiency and $^1O_2$ production of the HPRCs have been hypothesized to be the two-photon absorption property.

3.5. Two-Photon Absorption. TPACSs of HPRCs at 808 nm (σ_{808}) have been measured by the well-established method involving two-photon-induced fluorescence.[26] σ_{808} of HPRCs was 51−142 GM (1 GM = 10^{-50} cm^4 s photon^{-1}) as shown in Table 2, which was not only higher than the suggested value for optical imaging applications (0.1 GM)[27] but also higher than similar mononuclear Ru(II)[28,29] and Ir(III)[30] complexes at around 800 nm. Nevertheless, the σ_{808} values of HPRCs are lower than some dinuclear Ru(II),[12] Os(II),[13] and Ir(III)[26] complexes. **Ru1** showed the highest σ_{808}, which could explain its remarkable photodynamic activity ($\Phi_{\Delta 808}$) under 808 nm excitation.

3.6. Determination of *n*-Octanol and Water Distribution Coefficient. Investigation into the lipophilicity provides an important basis for cell membrane penetration, cellular uptake and bioavailability of drugs and reported polypyridyl Ru(II) complexes.[31−33] The distributions of **Ru1**−**Ru3** in *n*-octanol/water solutions were shown in Figure S10. The oil/water partition coefficients (log $K_{O/W}$) were determined by the concentrations of complexes in both phases. It is evident that these complexes have optimum lipophilic properties (log $K_{O/W}$ = 1.47−2.34), which would make them not only enter cells efficiently but also have significant benefits in the process of pharmaceutical application, such as balanced volume of distribution and potential for good absorption and bioavailability.

3.7. Mitochondrial Colocalization. The subcellular target is crucial for the activity and mechanism of drugs.[34] The subcellular colocalization of **Ru1**−**Ru3** with the mitochondria dye MitoTracker Green (MTG) was explored by CLSM on A375 human melanoma cells. All HPRCs showed weak luminescence within the cells under two-photon excitation at 808 nm (Figure 5a), which almost coincided with the signals of MTG but overlapped poorly with the nuclei dye Hoechst33324. The high Pearson's correlation coefficients (R) for the colocalization between MTG and HPRCs indicate that the complexes preferentially accumulate in the mitochondria. Their impermeable nature to the nucleus membrane or their low affinities for nuclear DNA could be factors impeding their

https://doi.org/10.1021/acs.inorgchem.3c00585
Inorg. Chem. 2023, 62, 8210−8218

Table 2. Singlet Oxygen Quantum Yield at 450 nm ($\Phi_{\Delta 450}$) and 808 nm ($\Phi_{\Delta 808}$), Two-Photon Absorption Cross-Section at 808 nm (σ_{808}, GM) In Vitro (Photo)Cytotoxicity (IC_{50}, μM) and Phototherapy Index (PI) of Ru1−Ru3 toward Thick-Bedded A375 Human Melanoma Cell Lines

complex	$\Phi_{\Delta 450}$	$\Phi_{\Delta 808}$	σ_{808}	$IC_{50,\ dark}$	$IC_{50,\ 450}$	PI-1	$IC_{50,\ 808}$	PI-2
Ru1	0.59	0.11	142	>200	0.726 ± 0.070	>275	0.513 ± 0.042	>390
Ru2	0.13	0.04	51	>200	53.6 ± 4.8	>3.73	34.1 ± 2.9	>5.87
Ru3	0.49	0.08	97	>200	2.75 ± 0.26	>72.7	2.51 ± 0.18	>79.7
Ru0	0.13	0.05	91	28.6 ± 2.4	5.36 ± 0.48	5.33	4.65 ± 0.37	6.15

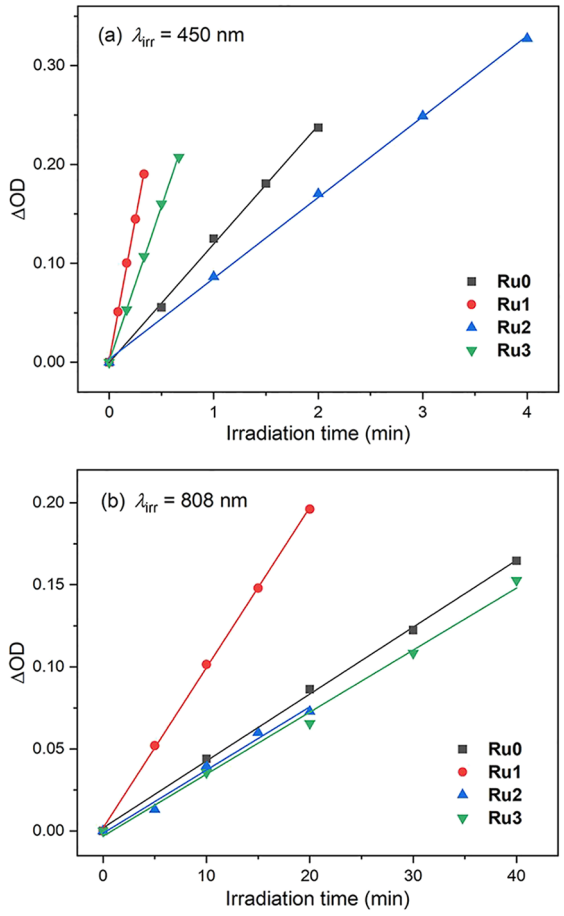

Figure 4. Measurement of singlet oxygen quantum yield of HPRCs by ABDA in aqueous solution upon 450 nm LED (50 mW cm^{-2}) and 808 nm LPL (100 mW cm^{-2}) irradiation.

effective accumulation in the nuclei. As a result, mitochondria become the primary target of **Ru1−Ru3**, consistent with some Ru(II) complexes which were reported to be mitochondria-targeted and challenging to enter the nucleus.[35,36]

3.8. Cell Uptake. Cell uptake and intracellular distribution of **Ru1−Ru3** was further tested by ICP-MS (Figure 5b). The cell uptake amounts of HPRCs are very comparable to typical metal complexes.[37] The cytoplasm and nucleus contain 96.2 and 3.1% of the whole cell's ruthenium, respectively, while 92.3% of the ruthenium in the whole cell has been found in the mitochondrion. The uptake of HPRC by A375 cells exhibited clear concentration dependence (Figure S12). This further demonstrates the mitochondrial selectivity of HPRCs and their effective cell uptake capacity. The amount of HPRCs taken up by cells also showed a positive correlation with their hydrophobicity (**Ru1** > **Ru3** > **Ru2**). Therefore, the optimized lipophilicity of **Ru1−Ru3** is beneficial to their efficient cell uptake.[33]

3.9. Intracellular $^1O_2$ Generation. Given that the HPRCs possess efficient cell uptake and high $^1O_2$ yields in the aqueous solution upon both VIS and IR light irradiations, their intracellular $^1O_2$ generation abilities have been studied (Figure 5c) by the well-established DCFH-DA method. After either 450 or 808 nm irradiation, all HPRCs induced bright luminescence of DCF over the entire cell, demonstrating the intracellular production of ROS. In the presence of $^1O_2$ scavenger ABDA, no ROS generated in the complex-treated A375 cells under the same TP irradiation (Figure S11), indicating $^1O_2$ is the main species in the photogenerated ROS by the HPRCs. Not surprisingly, **Ru1** exhibited the most potent intracellular $^1O_2$ production, as it did in an aqueous solution. This can provide substantial support for the HPRCs to become effective PS for antitumor PDT.

3.10. Cytotoxicity to Cancerous Cells. The cytotoxicities of HPRCs **Ru1−Ru3** and **Ru0** on the human melanoma cells A375 were evaluated by CCK-8 assay (Table 2). Under the dark condition, **Ru1−Ru3** showed negligible cytotoxicity at a concentration of 200 μM. Their half-maximal inhibitory concentrations in the dark ($IC_{50,\ dark}$) were expressed as >200 μM. This dark toxicity is apparently lower than most recently reported PSs based on transition metal complexes, such as hydrolysable $[RuL_2Cl_2]$-type complexes (<5 μM),[4] cyclometalated Pt(II) complexes (~17 μM),[38] self-assembly arene-Ru(II) complexes,[39] bis-terpyridyl Ru(II) complexes,[40] and is similar to Ir-bodipy complexes,[41] Ru-bodipy complexes,[42] and HPRCs $[Ru(dppz\text{-}X_2)_3]^{2+}$ based on classic dppz-type ligand (>100 μM).[43] Upon irradiation with the 450 nm LED array and 808 nm LPL, the HPRCs, especially **Ru1**, induced remarkable cell death ($IC_{50,\ 450}$ = 0.726 ± 0.070 μM and $IC_{50,\ 808}$ = 0.513 ± 0.042 μM). The phototherapy indexes under 450 (PI-1) and 808 nm (PI-2) for **Ru1** reached as high as >275 and > 390, respectively, indicating that it is an IR-excitable PS for antitumor PDT. Both PI-1 and PI-2 of HPRCs are significantly high among metal-containing PSs summarized in recent reviews (typically <100).[3,5,6,44−49] The phototoxicity of HPRCs $[Ru(dppz\text{-}X_2)_3]^{2+}$ have been reported to decrease as their lipophilicity increases.[43] Quite the contrary, for HPRCs in this work, a decrease in lipophilicity leads to an apparent reduction in phototoxicity. The high activity of **Ru1** is attributed to its enhanced cell uptake, brought about by its higher lipophilicity, and its greater photoexcited $^1O_2$ yield. The disparity in the structure−activity relationship of various series of HPRCs underlines a demand for more broad and in-depth research.

In stark contrast to HPRC, **Ru0** showed moderate toxicity to A375 cells without irradiation, similar to previously observed in other tumor cell lines,[16] and the cytotoxicity was less improved under 450 or 808 nm irradiation. It demonstrated that replacing the auxiliary ligands bpy in **Ru0** with sip-type ligands reduced the dark toxicity (chemotherapy toxicity) and increased the photocytotoxicity. **Ru0** has very high DNA affinity via intercalation mode, while the HPRCs are not potent DNA

https://doi.org/10.1021/acs.inorgchem.3c00585
Inorg. Chem. 2023, 62, 8210−8218

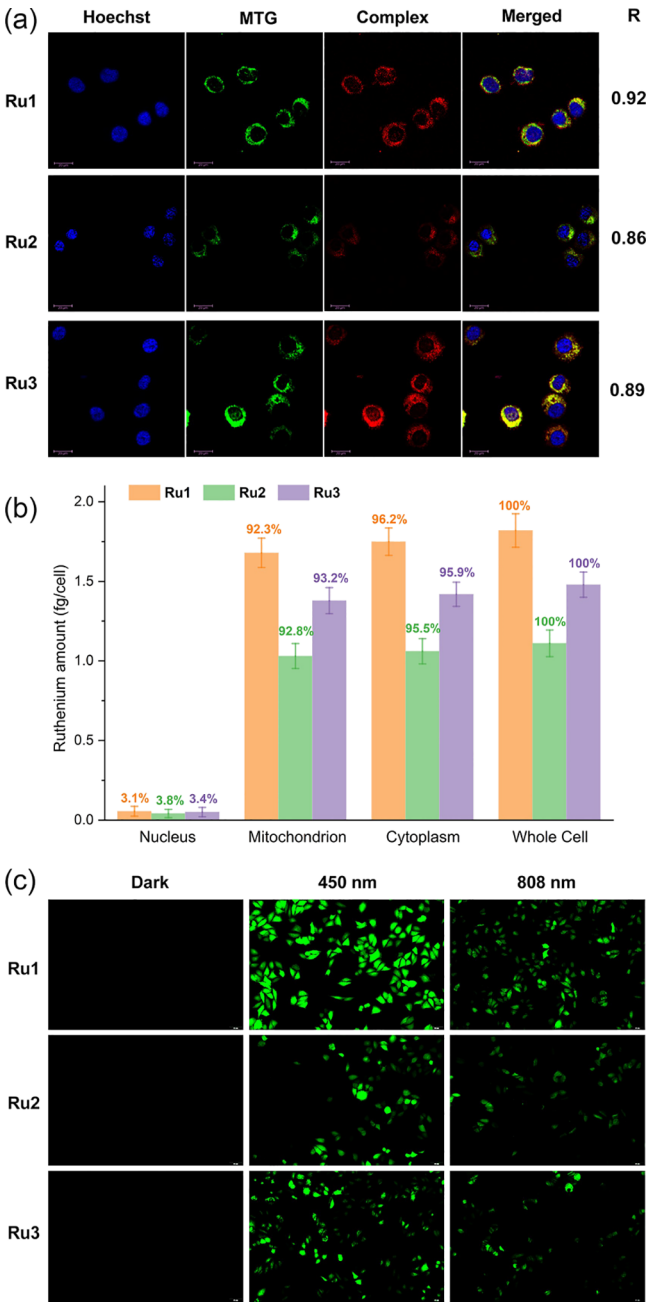

Figure 5. Colocalization of HPRCs with mitochondria (stained by MTG) in A375 cells by CLSM for **Ru1**−**Ru3** (a) and Ru distribution for **Ru1**−**Ru3** in different parts of the cell by ICP-MS (b), as well as DCFH-DA detection of intracellular $^1O_2$ generation for **Ru1**−**Ru3** (5 μM) upon 450 nm LED (50 mW cm^{-2}) and 808 nm LPL (100 mW cm^{-2}) irradiation for 5 min (c). Nuclei were stained by Hoechst 33324 (Hoechst). Pearson's correlation coefficients (R) were calculated for the colocalization between MTG and HPRCs. The percentages represent the relative contents of Ru in each examined part of the whole cell.

binders as revealed by the slight changes in absorption spectral titration (Figure S13) and the small DNA melting point increases in DNA denaturation (Figure S14). The possible factors may be the steric hindrance of large auxiliary ligands. The enhanced $^1O_2$ quantum yields by introducing two more sip-type ligands greatly boost their DNA photocleavage activities (Figure S15) and photocytotoxicities.

3.11. Apoptosis Assay. Flow cytometry detection of apoptosis in A375 cells, stained with Annexin V-FITC (AV) and PI (Figures 6a and S16), has been further carried out for the

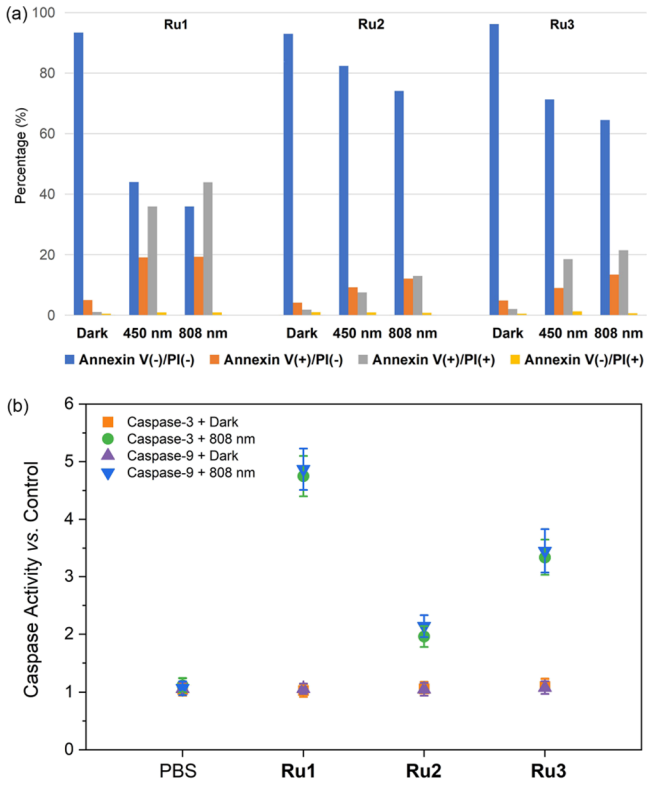

Figure 6. Photoinduced A375 cell apoptosis and caspase activation by **Ru1**−**Ru3**. (a) Flow cytometry detection of apoptosis in A375 cells (stained with Annexin V-FITC and PI) for the PDT treatments of HPRCs (1 μM) in the dark or upon 450 nm LED (50 mW cm^{-2}) and 808 nm LPL (100 mW cm^{-2}) irradiation. (b) Caspase-9 and -3 activities in A375 cells in the presence of HPRC (1 μM) in the dark or upon 808 nm LPL irradiation (100 mW cm^{-2}).

PDT treatments of **Ru1**−**Ru3**. The proportions of necrotic cells (Q1) were ignorable during the assay. In the absence of light, less than 2% of the HPRC-treated cells were found in the apoptotic stage (Q2), which is close to the number of cells in the blank group (A375 cells alone). It indicated that the HPRCs have minimal apoptosis-inducing activity in the dark. Upon light irradiation, the apoptotic rates of the HPRC-treated cells increased, especially for **Ru1**. Therefore, the remarkable in vitro phototherapy efficacy of **Ru1** is primarily a result of the apoptotic pathway induced by light-generated singlet oxygen.

HPRC-treated A375 cells stained by AV alone were also analyzed to confirm whether the flow cytometry results were affected by the emission of HPRCs as their emission maximums were very close to PI. The percentages of apoptotic cells represented by the AV signals (Figure S17a), both in the dark and upon irradiation, were almost identical to the total apoptosis rates indicated in the AV/PI analysis (Figure 6a). An additional PI channel detection of A375 cells treated by HPRC alone (without PI in the dark) and stained by PI alone was also performed (Figure S17b). The results indicated that the fluorescence of HPRC-treated cells had only a slight influence on the PI signals for the judgment of cell apoptosis. Although HPRCs emit in anhydrous organic solvents, their aqueous solutions were almost non-emissive due to the quenching effect

https://doi.org/10.1021/acs.inorgchem.3c00585
Inorg. Chem. 2023, 62, 8210−8218

of water molecules (Figure S18). Based on the protection of DNA base pairs, classic DNA-intercalative Ru(II) complexes and organic dyes can recover their emission and serve as DNA light switches. For HPRCs, their emissions after binding to DNA were nearly the same as free HPRCs (Figure S18), suggesting that they were still quenchable by water molecules, most probably via the two sip ligands outside. Therefore, the signals detected in flow cytometry under the concentrations in this study almost entirely came from the DNA-bound PI and were not interfered with by the Ru(II) complexes.

In the apoptotic process, caspase-9 propagates a cascade of further caspase processing events by directly cleaving and activating caspase-3 and caspase-7 to execute cell death. Caspase-9 and -3 activities were measured in the HPRC-treated A375 cells (Figure 6b). All complexes exhibited no caspase-9 or -3 activation under dark conditions. With 808 nm LPL irradiation, both caspase-9 and -3 activities rose substantially. These findings demonstrate that the HPRCs initiate a photo-depended apoptosis mechanism.

3.12. Cytotoxicity to Noncancerous Cells. The toxicity of PS to normal cells is one of the most commonly observed undesired effects of PDT in clinical settings. The cytotoxicities of HPRCs **Ru1**−**Ru3** and **Ru0** to the human normal liver (HL-7702) cells were tested using cell viability incubated with different concentrations of Ru(II) complexes (Figure S18). **Ru0** showed low toxicity to HL-7702 cells. At a concentration around the IC_{50} for phototherapy in A375 cells (5.0 μM), **Ru0** reduced HL-7702 cell viability by less than 10%. Despite a 10-fold increase in **Ru0** concentration (50 μM), the HL-7702 cell viability was still 67%. The toxicities of **Ru1**−**Ru3** to normal cells were even lower than that of **Ru0**. For **Ru1**, the HL-7702 cell viability was higher than 95% when the concentration reached 5.0 μM (10 times higher than its phototherapeutic IC_{50}). The low cytotoxicity of HPRCs to normal cells greatly increased their potential as high-selective and safe PSs for antitumor PDT.

4. CONCLUSIONS

In summary, a series of homoligand polypyridyl ruthenium complexes ($[Ru(L)_3]^{2+}$) containing three singlet oxygen-generating ligands (L) in a single molecule have been constructed. The complexes exhibited significantly enhanced $^1O_2$ quantum yield compared to their heteroligand parents, under the irradiation of both visible light (450 nm) and infrared light (808 nm) by one- and two-photon absorption, respectively. The HPRCs target the mitochondria but not the nuclei. **Ru1** has a remarkable phototherapy index for human malignant melanoma cells upon irradiation of 808 nm low-power laser and very low toxicity to human normal liver cells, suggesting its high potential as IR-excitable antitumor PDT reagent with improved therapeutic efficacy and safety. We expect that our study on the two-photon antitumor PDT activity of HPRC will pique the attention of those working in chemistry, pharmacy, optical materials, and other relevant domains in homoligand metal complexes.

■ ASSOCIATED CONTENT

Supporting Information

The Supporting Information is available free of charge at https://pubs.acs.org/doi/10.1021/acs.inorgchem.3c00585.

Synthesis and characterizations, simulated and experimental absorption spectra, photostability, plots of excited states transitions, DNA-binding experiments, quantum yield determination for the $^1O_2$ generation, DNA photocleavage, oil/water partition, experimental and computational absorption spectral data of HPRCs (PDF)

■ AUTHOR INFORMATION

Corresponding Author

Feng Gao − *Key Laboratory of Medicinal Chemistry for Natural Resource, Ministry of Education; Yunnan Provincial Center for Research & Development of Natural Products; School of Pharmacy, Yunnan University, Kunming 650500, P. R. China;* orcid.org/0000-0001-7490-4887; Email: gaofeng@ynu.edu.cn

Authors

Shi-Jie Tang − *Key Laboratory of Medicinal Chemistry for Natural Resource, Ministry of Education; Yunnan Provincial Center for Research & Development of Natural Products; School of Pharmacy, Yunnan University, Kunming 650500, P. R. China*

Meng-Fan Wang − *Key Laboratory of Medicinal Chemistry for Natural Resource, Ministry of Education; Yunnan Provincial Center for Research & Development of Natural Products; School of Pharmacy, Yunnan University, Kunming 650500, P. R. China*

Rong Yang − *Key Laboratory of Medicinal Chemistry for Natural Resource, Ministry of Education; Yunnan Provincial Center for Research & Development of Natural Products; School of Pharmacy, Yunnan University, Kunming 650500, P. R. China*

Meng Liu − *Key Laboratory of Medicinal Chemistry for Natural Resource, Ministry of Education; Yunnan Provincial Center for Research & Development of Natural Products; School of Pharmacy, Yunnan University, Kunming 650500, P. R. China*

Qing-Fang Li − *Key Laboratory of Medicinal Chemistry for Natural Resource, Ministry of Education; Yunnan Provincial Center for Research & Development of Natural Products; School of Pharmacy, Yunnan University, Kunming 650500, P. R. China*

Complete contact information is available at: https://pubs.acs.org/10.1021/acs.inorgchem.3c00585

Notes

The authors declare no competing financial interest.

■ ACKNOWLEDGMENTS

This work was supported by the National Natural Science Foundation of China (22167022), Yunnan Provincial Science and Technology Department (2018FB022), Youth Talents Project of Yunnan Province (QNBJ-2018-057). The authors thank the Advanced Analysis and Measurement Center of Yunnan University for their help in characterization.

■ REFERENCES

(1) Roque, J. A., III; Cole, H. D.; Barrett, P. C.; Lifshits, L. M.; Hodges, R. O.; Kim, S.; Deep, G.; Francés-Monerris, A.; Alberto, M. E.; Cameron, C. G.; McFarland, S. A. Intraligand Excited States Turn a Ruthenium Oligothiophene Complex into a Light-Triggered Ubertoxin with Anticancer Effects in Extreme Hypoxia. *J. Am. Chem. Soc.* **2022**, *144*, 8317−8336.

(2) Wu, Y.; Li, S.; Chen, Y.; He, W.; Guo, Z. Recent Advances of Noble Metal Complex based Photodynamic Therapy. *Chem. Sci.* **2022**, *13*, 5085−5106.

(3) Madec, H.; Figueiredo, F.; Cariou, K.; Roland, S.; Sollogoub, M.; Gasser, G. Metal complexes for catalytic and photocatalytic reactions in living cells and organisms. *Chem. Sci.* **2023**, *14*, 409−442.
(4) Wu, C.-Y.; Chen, H.-J.; Wu, Y.-C.; Tsai, S.-W.; Liu, Y.-H.; Bhattacharya, U.; Lin, D.; Tai, H.-C.; Kong, K. V. Highly Efficient Singlet Oxygen Generation by BODIPY−Ruthenium(II) Complexes for Promoting Neurite Outgrowth and Suppressing Tau Protein Aggregation. *Inorg. Chem.* **2023**, *62*, 1102−1112.
(5) Conti, L.; Macedi, E.; Giorgi, C.; Valtancoli, B.; Fusi, V. Combination of light and Ru(II) polypyridyl complexes: Recent advances in the development of new anticancer drugs. *Coord. Chem. Rev.* **2022**, *469*, No. 214656.
(6) Ma, Z.; Han, H.; Zhao, Y. Mitochondrial dysfunction-targeted nanosystems for precise tumor therapeutics. *Biomaterials* **2023**, *293*, No. 121947.
(7) McKenzie, L. K.; Bryant, H. E.; Weinstein, J. A. Transition metal complexes as photosensitisers in one- and two-photon photodynamic therapy. *Coord. Chem. Rev.* **2019**, *379*, 2−29.
(8) Monro, S.; Colon, K. L.; Yin, H. M.; Roque, J.; Konda, P.; Gujar, S.; Thummel, R. P.; Lilge, L.; Cameron, C. G.; McFarland, S. A. Transition Metal Complexes and Photodynamic Therapy from a Tumor-Centered Approach: Challenges, Opportunities, and Highlights from the Development of TLD1433. *Chem. Rev.* **2019**, *119*, 797−828.
(9) McGhie, B. S.; Aldrich-Wright, J. R. Photoactive and Luminescent Transition Metal Complexes as Anticancer Agents: A Guiding Light in the Search for New and Improved Cancer Treatments. *Biomedicines* **2022**, *10*, 578.
(10) Roque, J. A., 3rd; Barrett, P. C.; Cole, H. D.; Lifshits, L. M.; Shi, G.; Monro, S.; von Dohlen, D.; Kim, S.; Russo, N.; Deep, G.; Cameron, C. G.; Alberto, M. E.; McFarland, S. A. Breaking the barrier: an osmium photosensitizer with unprecedented hypoxic phototoxicity for real world photodynamic therapy. *Chem. Sci.* **2020**, *11*, 9784−9806.
(11) Roque, J. A., 3rd; Barrett, P. C.; Cole, H. D.; Lifshits, L. M.; Bradner, E.; Shi, G.; von Dohlen, D.; Kim, S.; Russo, N.; Deep, G.; Cameron, C. G.; Alberto, M. E.; McFarland, S. A. Os(II) Oligothienyl Complexes as a Hypoxia-Active Photosensitizer Class for Photodynamic Therapy. *Inorg. Chem.* **2020**, *59*, 16341−16360.
(12) Wang, M.-F.; Yang, R.; Tang, S.-J.; Deng, Y.-A.; Li, G.-K.; Zhang, D.; Chen, D.; Ren, X.; Gao, F. In vivo Realization of Dual Photodynamic and Photothermal Therapy for Melanoma by Mitochondria Targeting Dinuclear Ruthenium Complexes under Civil Infrared Low-power Laser. *Angew. Chem., Int. Ed.* **2022**, *61*, No. e202208721.
(13) Wang, M.-F.; Deng, Y.-A.; Li, Q.-F.; Tang, S.-J.; Yang, R.; Zhao, R.-Y.; Liu, F.-D.; Ren, X.; Zhang, D.; Gao, F. Dinuclear osmium complexes as mitochondrion-targeting antitumor photothermal agents in vivo. *Chem. Commun.* **2022**, *58*, 12676−12679.
(14) Hou, Z.; Deng, K.; Wang, M.; Liu, Y.; Chang, M.; Huang, S.; Li, C.; Wei, Y.; Cheng, Z.; Han, G.; Al Kheraif, A. A.; Lin, J. Hydrogenated Titanium Oxide Decorated Upconversion Nanoparticles: Facile Laser Modified Synthesis and 808 nm Near-Infrared Light Triggered Phototherapy. *Chem. Mater.* **2019**, *31*, 774−784.
(15) Bi, X.-D.; Yang, R.; Zhou, Y.-C.; Chen, D.; Li, G.-K.; Guo, Y.-X.; Wang, M.-F.; Liu, D.; Gao, F. Cyclometalated Iridium(III) Complexes as High-Sensitivity Two-Photon Excited Mitochondria Dyes and Near-Infrared Photodynamic Therapy Agents. *Inorg. Chem.* **2020**, *59*, 14920−14931.
(16) Ma, G.-L.; Bi, X.-D.; Gao, F.; Feng, Z.; Zhao, D.-C.; Lin, F.-J.; Yan, R.; Liu, D.; Liu, P.; Chen, J.; Zhang, H. Novel polypyridyl ruthenium complexes acting as high affinity DNA intercalators, potent transcription inhibitors and antitumor reagents. *J. Inorg. Biochem.* **2018**, *185*, 1−9.
(17) Chen, F.; Romero-Canelón, I.; Habtemariam, A.; Song, J.-I.; Banerjee, S.; Clarkson, G. J.; Song, L.; Prokes, I.; Sadler, P. J. Effect of cysteine thiols on the catalytic and anticancer activity of Ru(ii) sulfonyl-ethylenediamine complexes. *Dalton Trans.* **2022**, *51*, 4447−4457.
(18) Pradhan, A. K.; Shyam, A.; Dutta, A.; Mondal, P. Quantum Chemical Investigation on Hydrolysis of Orally Active Organometallic Ruthenium(II) and Osmium(II) Anticancer Drugs and Their Interaction with Histidine. *J. Phys. Chem. B* **2022**, *126*, 9516−9527.
(19) Pal, A. K.; Hanan, G. S. Design, synthesis and excited-state properties of mononuclear Ru(ii) complexes of tridentate heterocyclic ligands. *Chem. Soc. Rev.* **2014**, *43*, 6184−6197.
(20) Lifshits, L. M.; Roque Iii, J. A.; Konda, P.; Monro, S.; Cole, H. D.; von Dohlen, D.; Kim, S.; Deep, G.; Thummel, R. P.; Cameron, C. G.; Gujar, S.; McFarland, S. A. Near-infrared absorbing Ru(ii) complexes act as immunoprotective photodynamic therapy (PDT) agents against aggressive melanoma. *Chem. Sci.* **2020**, *11*, 11740−11762.
(21) Shahroosvand, H.; Abaspour, S.; Pashaei, B.; Radicchi, E.; De Angelis, F.; Bonaccorso, F. A ruthenium tetrazole complex-based high efficiency near infrared light electrochemical cell. *Chem. Commun.* **2017**, *53*, 6211−6214.
(22) Kaufmann, M.; Muller, C.; Cullen, A. A.; Brandon, M. P.; Dietzek, B.; Pryce, M. T. Photophysics of Ruthenium(II) Complexes with Thiazole pi-Extended Dipyridophenazine Ligands. *Inorg. Chem.* **2021**, *60*, 760−773.
(23) Ni, B.; Cao, H.; Zhang, C.; Li, S.; Zhang, Q.; Tian, X.; Li, D.; Wu, J.; Tian, Y. Activated Type I and Type II Process for Two-Photon Promoted ROS Generation: The Coordinated Zn Matters. *Inorg. Chem.* **2020**, *59*, 13671−13678.
(24) Li, J. A.; Zhou, J.; Mao, Z.; Xie, Z.; Yang, Z.; Xu, B.; Liu, C.; Chen, X.; Ren, D.; Pan, H.; Shi, G.; Zhang, Y.; Chi, Z. Transient and Persistent Room-Temperature Mechanoluminescence from a White-Light-Emitting AIEgen with Tricolor Emission Switching Triggered by Light. *Angew. Chem., Int. Ed.* **2018**, *57*, 6449−6453.
(25) Li, L. P.; Ye, B. H. Efficient Generation of Singlet Oxygen and Photooxidation of Sulfide into Sulfoxide via Tuning the Ancillary of Bicyclometalated Iridium(III) Complexes. *Inorg. Chem.* **2019**, *58*, 7775−7784.
(26) Xu, W. J.; Liu, S. J.; Zhao, X.; Zhao, N.; Liu, Z. Q.; Xu, H.; Liang, H.; Zhao, Q.; Yu, X. Q.; Huang, W. Synthesis, One- and Two-Photon Photophysical and Excited-State Properties, and Sensing Application of a New Phosphorescent Dinuclear Cationic Iridium(III) Complex. *Chem. − Eur. J.* **2013**, *19*, 621−629.
(27) Furuta, T.; Wang Samuel, S. H.; Dantzker Jami, L.; Dore Timothy, M.; Bybee Wendy, J.; Callaway Edward, M.; Denk, W.; Tsien Roger, Y. Brominated 7-hydroxycoumarin-4-ylmethyls: Photolabile protecting groups with biologically useful cross-sections for two photon photolysis. *Proc. Natl. Acad. Sci. U. S. A.* **1999**, *96*, 1193−1200.
(28) Castellano, F. N.; Malak, H.; Gryczynski, I.; Lakowicz, J. R. Creation of Metal-to-Ligand Charge Transfer Excited States with Two-Photon Excitation. *Inorg. Chem.* **1997**, *36*, 5548−5551.
(29) Boca, S. C.; Four, M.; Bonne, A.; van der Sanden, B.; Astilean, S.; Baldeck, P. L.; Lemercier, G. An ethylene-glycol decorated ruthenium-(ii) complex for two-photon photodynamic therapy. *Chem. Commun.* **2009**, *30*, 4590−4592.
(30) Edkins, R. M.; Bettington, S. L.; Goeta, A. E.; Beeby, A. Two-photon spectroscopy of cyclometalated iridium complexes. *Dalton Trans.* **2011**, *40*, 12765−12770.
(31) Poynton, F. E.; Bright, S. A.; Blasco, S.; Williams, D. C.; Kelly, J. M.; Gunnlaugsson, T. The development of ruthenium(ii) polypyridyl complexes and conjugates for in vitro cellular and in vivo applications. *Chem. Soc. Rev.* **2017**, *46*, 7706−7756.
(32) Puckett, C. A.; Ernst, R. J.; Barton, J. K. Exploring the cellular accumulation of metal complexes. *Dalton Trans.* **2010**, *39*, 1159−1170.
(33) Puckett, C. A.; Barton, J. K. Methods to explore cellular uptake of ruthenium complexes. *J. Am. Chem. Soc.* **2007**, *129*, 46−47.
(34) Mulcahy, S. P.; Gründler, K.; Frias, C.; Wagner, L.; Prokop, A.; Meggers, E. Discovery of a strongly apoptotic ruthenium complex through combinatorial coordination chemistry. *Dalton Trans.* **2010**, *39*, 8177−8182.
(35) Yu, Q.; Liu, Y.; Xu, L.; Zheng, C.; Le, F.; Qin, X.; Liu, Y.; Liu, J. Ruthenium(II) polypyridyl complexes: Cellular uptake, cell image and apoptosis of HeLa cancer cells induced by double targets. *Eur. J. Med. Chem.* **2014**, *82*, 82−95.
(36) Paul, S.; Kundu, P.; Bhattacharyya, U.; Garai, A.; Maji, R. C.; Kondaiah, P.; Chakravarty, A. R. Ruthenium(II) Conjugates of Boron-

https://doi.org/10.1021/acs.inorgchem.3c00585
Inorg. Chem. 2023, 62, 8210−8218

Dipyrromethene and Biotin for Targeted Photodynamic Therapy in Red Light. *Inorg. Chem.* **2020**, *59*, 913−924.
(37) Shum, J.; Leung, P. K.-K.; Lo, K. K.-W. Luminescent Ruthenium(II) Polypyridine Complexes for a Wide Variety of Biomolecular and Cellular Applications. *Inorg. Chem.* **2019**, *58*, 2231−2247.
(38) Liu, Y.; Zhao, H.; Li, L.; Yang, B.; Yue, Y.; Li, M.; Shi, X.; Zhang, B.; Wang, L.; Qi, C.; Liu, Y.; Ren, S.; Zhang, K.; Yoon, J. A tyrosinase-activated Pt(II) complex for melanoma photodynamic therapy and fluorescence imaging. *Sens. Actuators, B* **2023**, *374*, No. 132836.
(39) Xu, G.; Li, C.; Chi, C.; Wu, L.; Sun, Y.; Zhao, J.; Xia, X.-H.; Gou, S. A supramolecular photosensitizer derived from an Arene-Ru(II) complex self-assembly for NIR activated photodynamic and photothermal therapy. *Nat. Commun.* **2022**, *13*, 3064.
(40) Liu, B.; Gao, Y.; Jabed, M. A.; Kilina, S.; Liu, G.; Sun, W. Lysosome Targeting Bis-terpyridine Ruthenium(II) Complexes: Photophysical Properties and In Vitro Photodynamic Therapy. *ACS Appl. Bio Mater.* **2020**, *3*, 6025−6038.
(41) Liu, C.; Jiang, Y.; Xiang, J.; Xiang, C.; Li, H.; Li, H.; Wei, F.; Huang, J.; Li, R.; Man-Chung Wong, K.; Gong, P. Development of Bodipy-Ir complex as an near-infrared photosensitizer for photoacoustic imaging-guided photodynamic therapy. *Dyes Pigm.* **2023**, *209*, No. 110900.
(42) Paul, S.; Kundu, P.; Kondaiah, P.; Chakravarty, A. R. BODIPY-Ruthenium(II) Bis-Terpyridine Complexes for Cellular Imaging and Type-I/-II Photodynamic Therapy. *Inorg. Chem.* **2021**, *60*, 16178−16193.
(43) Roy, S.; Colombo, E.; Vinck, R.; Mari, C.; Rubbiani, R.; Patra, M.; Gasser, G. Increased Lipophilicity of Halogenated Ruthenium(II) Polypyridyl Complexes Leads to Decreased Phototoxicity in vitro when Used as Photosensitizers for Photodynamic Therapy. *ChemBioChem* **2020**, *21*, 2966−2973.
(44) Kar, B.; Das, U.; Roy, N.; Paira, P. Recent advances on organelle specific Ru(II)/Ir(III)/Re(I) based complexes for photodynamic therapy. *Coord. Chem. Rev.* **2023**, *474*, No. 214860.
(45) Paprocka, R.; Wiese-Szadkowska, M.; Janciauskiene, S.; Kosmalski, T.; Kulik, M.; Helmin-Basa, A. Latest developments in metal complexes as anticancer agents. *Coord. Chem. Rev.* **2022**, *452*, No. 214307.
(46) Ma, L.; Wang, Y.; Wang, X.; Zhu, Q.; Wang, Y.; Li, L.; Cheng, H.-B.; Zhang, J.; Liang, X.-J. Transition metal complex-based smart AIEgens explored for cancer diagnosis and theranostics. *Coord. Chem. Rev.* **2022**, *473*, No. 214822.
(47) Lee, L. C.-C.; Lo, K. K.-W. Luminescent and Photofunctional Transition Metal Complexes: From Molecular Design to Diagnostic and Therapeutic Applications. *J. Am. Chem. Soc.* **2022**, *144*, 14420−14440.
(48) Ankathatti Munegowda, M.; Manalac, A.; Weersink, M.; McFarland, S. A.; Lilge, L. Ru(II) containing photosensitizers for photodynamic therapy: A critique on reporting and an attempt to compare efficacy. *Coord. Chem. Rev.* **2022**, *470*, No. 214712.
(49) Banerjee, S. Polypyridyl Ruthenium(II) Complexes with Red-Shifted Absorption: New Promises in Photodynamic Therapy. *ChemBioChem* **2021**, *22*, 2407−2409.

https://doi.org/10.1021/acs.inorgchem.3c00585
Inorg. Chem. 2023, 62, 8210−8218